Article

The Effect of Cu^{2+} and Pb^{2+} in the Feed Solution on the Water and Reverse Solute Fluxes in the Forward Osmosis (FO) Process Using Nanofiltration (NF) Membranes

Amirsajad Atashgar, Daryoush Emadzadeh and Boguslaw Kruczek *

Department of Chemical and Biological Engineering, University of Ottawa, Ottawa, ON K1N 6N5, Canada;
aatas086@uottawa.ca (A.A.); demadzad@uottawa.ca (D.E.)
* Correspondence: bkruczek@uottawa.ca

Abstract: The application of nanofiltration (NF) membranes in the forward osmosis (FO) process to remove heavy metal ions from wastewater is an emerging concept. Unlike NF, FO does not require an external driving force. Although the product, a dilute draw solution, must further be processed by NF to produce pure water and reconcentrate a draw solution, the feed to that NF process is "clean", which minimizes membrane fouling. This paper examines the role of Cu^{2+} and Pb^{2+} in the feed solution on the water and the reverse solute fluxes in FO process using novel thin film nanocomposite (TFN) NF membranes. The TFN membranes were fabricated by in situ interfacial polymerization of piperazine (PIP) and 1,3,5-benzenetricarbonyl trichloride (TMC) containing different amounts of dispersed halloysite nanotubes (HNTs) nanoparticles functionalized with the first generation of poly(amidoamine) (PAMAM) dendrimers. The presence of Cu^{2+} and Pb^{2+} in the feed solution decreased the reverse flux of MgCl$_2$ by at least 2.5 times compared to the experiments with pure water as a feed. Simultaneously, the water flux also increased. The corresponding rejections of Cu^{2+} and Pb^{2+} in the FO process ranged from 94.5% to 98.1%.

Keywords: forward osmosis; heavy metal removal; TFN membranes; halloysite nanotubes; first generation of poly(amidoamine) dendrimers

1. Introduction

With fast industrialization, the discharge of wastewater containing heavy metals into the environment is increasing [1]. The term "heavy metals" has been criticized because of inconsistent definitions, and the International Union for Pure and Applied Chemistry (IUPAC) has repeatedly called to stop using it, without much success [2]. In the context of this research, heavy metals are elements with an atomic mass between 63.5 and 200.6 and a specific gravity of more than five [3]. Examples of heavy metals include zinc (Zn), copper (Cu), nickel (Ni), and lead (Pb). Heavy metals at low concentrations are vital for living organisms, including humans. However, at higher concentrations, they become toxic and harmful. For example, zinc is crucial for human health and vital for the physiological functions of living tissue, but too much zinc can cause severe health problems, including skin irritation, vomiting, and nausea. Copper is essential for animal metabolism. However, copper's excessive ingestion can create toxicological problems such as cramps, vomiting, and even death. Nickel is known as a human carcinogen; it can also damage the kidneys and lungs. Because heavy metals are not biodegradable, they must be removed from wastewater [3,4].

Different methods to remove heavy metals from wastewater include chemical precipitation, adsorption, ion exchange, coagulation-flocculation, solvent extraction, catalysis, bioremediation, and membrane separation. Several excellent review articles exist on heavy metal removal from wastewater [5–8]. Among different methods, adsorption has attracted the most attention, followed by membrane separation and ion exchange [8]. Each method

has its pros and cons. For example, the most popular adsorption methods offer flexible design and operation, are generally low-cost, and do not impose environmental risk. However, their efficiency and selectivity depend on the adsorbent selection. Also, the recovery of adsorbed heavy metal(s) requires an additional step—a desorption process [9]. In contrast, the ion exchange methods allow for easy metal recovery and are inherently highly efficient, but their selectivity depends on the chosen resin. Also, ion exchange methods are not easily scalable and require a pretreatment step [10]. On the other hand, membrane separation processes are highly efficient and selective, offer easy metal recovery and are easy to scale up. The major disadvantage of membrane processes is membrane fouling, which may require frequent membrane replacement and high capital costs [4].

Among different membrane separation processes, nanofiltration (NF) is most feasible for heavy metal removal from wastewater [11]. NF membranes have a small pore size (1–10 nm) that allows for direct application for heavy metal removal [12]. The NF is a pressure-driven membrane process in which separation relies on size exclusion and the Donnan potential [13]. The NF processes require the application of external pressure. The higher the pressure, the higher the energy consumption, which increases the process's operating cost. Furthermore, pressure-driven processes' membranes, including NF membranes, are susceptible to fouling, significantly reducing the membrane's lifespan [14].

The NF membranes can be used in forward osmosis (FO) processes [15]. Compared to pressure-driven membrane processes, FO is a relatively new membrane technology with potential applications in desalination, wastewater treatment and reclamation, bioproducts and food industry, energy generation, and resource recovery [16,17]. FO utilizes the osmotic pressure difference of solutions across a semipermeable membrane to draw water from a dilute feed solution (FS) to a more concentrated draw solution (DS); the salt moves in the opposite direction. Without external pressure, the fouling tendency of FO membranes is significantly reduced [18,19]. However, the FO is generally not a standalone process; it must be combined with another process. An example of a hybrid FO-NF process for heavy metal removal is shown in Figure 1. Heavy metals are rejected in the FO process. At the same time, water permeates from the feed to the draw solution. Therefore, the permeating water in the FO process is not the final product as it dilutes the draw solution. The purpose of the second stage, an NF process, is to regenerate the draw solution while producing pure water. The advantage of a hybrid process arises from using a "clean" draw solution rather than direct "dirty" wastewater in the NF process, which minimizes membrane fouling.
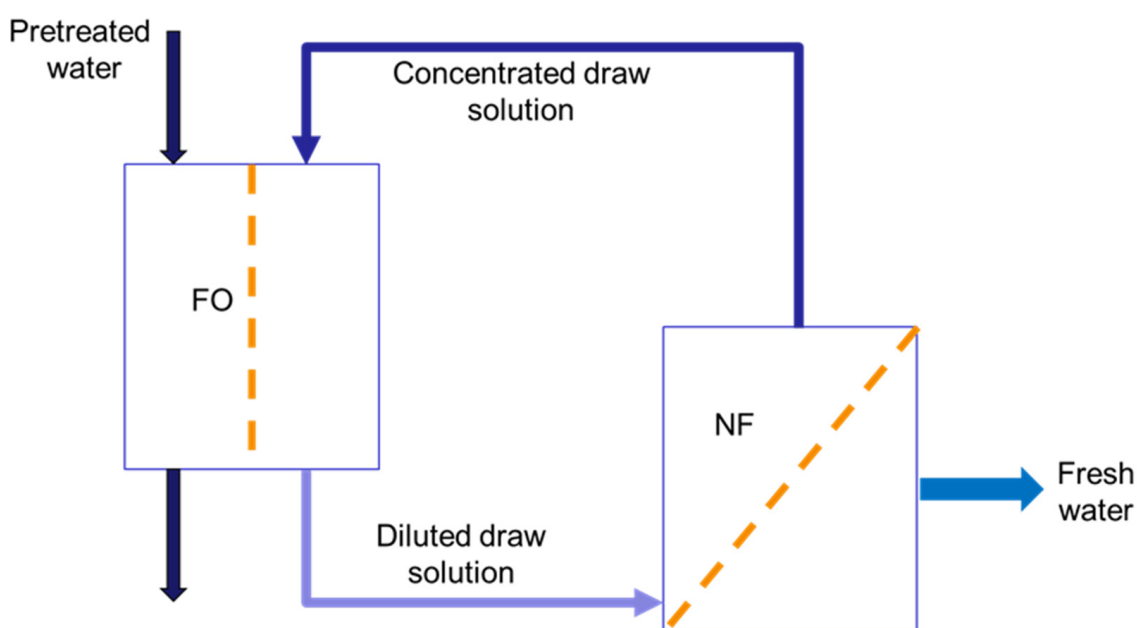

Figure 1. A hybrid two-stage FO-NF process for heavy metal removal from wastewater.

The membranes for the FO and NF steps in Figure 1 could be the same. If the NF-stage membrane effectively rejects the draw solute, it will also prevent reverse draw solute transport in the FO-stage. Therefore, the membranes for the first stage in Figure 1 are often referred to as "NF-like FO" membranes [15]. The hybrid process in Figure 1 can also be used for water desalination. However, since monovalent salts (e.g., NaCl) are to be rejected in the FO stage, the process would require an RO membrane or "RO-like FO" membrane [20]. Heavy metals occur as multivalent salts; it is thus sufficient to use NF-like FO membranes for heavy metal removal from wastewater. Moreover, NF-like FO membranes could achieve higher water flux than RO-like FO membranes due to a looser selective layer [21].

There is an increasing number of examples of NF-like FO applications. Abdullah et al. used commercial NF membranes in PRO and FO processes for treating aerobically treated palm oil mill effluent (AT-POME). They reported that the color (i.e., impurity) of AT-POME could be removed entirely using magnesium chloride ($MgCl_2$) as a draw solution [22]. The same research group also used four commercial NF membranes in the FO and PRO processes for copper ion removal from wastewater. They reported the near-complete removal of copper, regardless of the membrane type and membrane orientation associated with low reverse draw-solute flux [15]. Setiawan et al. tested different types of in-house-made NF hollow fire membranes in the FO process with pure water as a feed and 0.5 mol L^{-1} $MgCl_2$ as a draw solution. They reported a water flux as high as 9.74 $L \cdot m^{-2} \cdot h^{-1}$ [23]. Su et al. developed cellulose acetate-based NF membranes and studied the effect of draw solution concentration and membrane orientation (PRO vs. FO) on the water flux. Using 0.5–2.0 mol L^{-1} of $MgCl_2$ as a draw solution, they reported a higher water flux in the PRO mode (2.7–7.3 $L \cdot m^{-2}$ h^{-1}) than in the FO mode (1.8–5.0 $L \cdot m^{-2}$ h^{-1}) [9]. However, the role of heavy metal ions in the feed solution on the FO performance has not been systematically studied. More specifically, do heavy metal ions suppress, enhance, or not affect the water flux and the reverse solute flux?

This paper compares the FO performance of the TFN-NF membranes using deionized water and the respective aqueous solution of Cu^{2+} and Pb^{2+} as a feed. In all cases, aqueous $MgCl_2$ was used as a draw solution. The TFN membranes in this study utilized modified halloysite nanotubes (HNTs) as nanoparticles. More specifically, HNTs were functionalized with the first generation of poly(amidoamine) (PAMAM) dendrimers, and the resulting nanoparticles, HNTs-G1, were dispersed in the TMC monomer solution before interfacial polymerization [24]. The observed increase in the water flux combined with a significant reduction in the reverse solute flux in the presence of heavy metal ions was attributed to their adsorption by negatively charged TFN-NF membrane surface. To our knowledge, this is the first systematic study on the role of Cu^{2+} and Pb^{2+} in the feed solution on the water and the reverse solute fluxes of NF membranes used in the FO process.

2. Materials and Methods

2.1. Materials

The synthesis of HNTs-G1 that were used to fabricate TFN membranes was a multi-step process. First, HNTs were treated with a concentrated aqueous HCl solution and washed with distilled water to remove contaminants such as iron. Following that, the purified HNTs were amino-functionalized using aminopropyltriethoxysilane (APTES). The amino-functionalized HNTs (HNT-NH_2) were then reacted with methyl acrylate (MA) in ethanol solution (Michael reaction), followed by amidation of the ester groups with ethylene diamine. The nanoparticles were separated by centrifugation, and the resulting HNT-G1 was washed with distilled water and dried. The details of the synthesis of HNT-G1 are described elsewhere [25].

TFN membranes were prepared using four different loadings of HNTs-G1, 0, 0.025, 0.05, and 0.1%, where 0% loading corresponds to the control TFC membranes. The TFN membranes are coded as TFN (x%), where x corresponds to the loading of HNTs-G1. The nanoparticles were dispersed in the solution of 1,3,5-benzenetricarbonyl trichloride (TMC)

in n-hexane before the interfacial polymerization with the aqueous solution of piperazine (PIP). A commercial PS35 ultrafiltration (UF) membrane was used as a substrate for the interfacial polymerization of two monomer solutions. The details of the synthesis protocol of TFN membranes are described elsewhere [24].

Laboratory-grade copper (II) sulphate pentahydrate ($CuSO_4 \cdot 5H_2O$) and lead (II) nitrate ($Pb(NO_3)_2$) for the synthetic feed solutions, and magnesium chloride ($MgCl_2$) for the draw solution, were purchased from Sigma-Aldrich, Saint Louis, MO, USA. Deionized (DI) water was used to prepare the feed and draw solutions.

2.2. Nanoparticle and Membrane Characterization

Functionalized and pristine HNTs, and fresh TFN and TFC membranes, were thoroughly characterized using scanning electron microscopy (SEM) and attenuated total reflection-Fourier transform infrared (ATR-FTIR) spectroscopy. In addition, the contact angle and zeta potential of the surface of the membranes were determined. The results of these characterizations are described elsewhere [17] and will be briefly summarized in the next section.

The zeta potential of the surface of membranes was measured by a zeta analyzer (Zetasizer PSS0012-22, Malvern Instruments, Malvern, UK) before and after the tests with heavy metals. The measurements were carried out at neutral pH (6.5–7.0), which was the pH of the feed solution in all membrane performance tests. The adsorption of heavy metals on the membrane surface was evaluated using Agilent 7900 inductively-coupled plasma mass spectrometer (ICP-MS Aligent, Santa Clara, CA, USA). The same instrument was also used to determine the concentration of the heavy metals in the feed and draw solutions.

2.3. Forward Osmosis Tests and Data Analysis

The performance of TFN and the control TFC membranes was evaluated in our novel crossflow FO testing system, which is described in detail elsewhere [26]. The new feature of the FO system is bypass lines that allow for the isolation of the membrane cell from the rest of the system. In turn, it allows for a sudden replacement of DI water at both sides of the membrane with a desired feed and/or draw solution, which initiates the actual FO experiment [27]. During each experiment, the mass of the tanks containing the feed and draw solution is monitored in real-time using high-resolution (0.01 g) balances (6202-1S, Entris Precision, Sartorius, Germany). Also, the conductivity and temperature in the feed tank solution are monitored continuously using a benchtop conductivity/temperature meter (CON2700, Oakton Instruments, Woonsocket, RI, USA). The membranes were tested in the orientation of the active layer facing feed solution (AL-FS). We used the same draw solution in all experiments, i.e., 1 M $MgCl_2$ aqueous solution. For the feed solution, we used either DI water or 200 ppm solutions of $CuSO_4 \cdot 5H_2O$ or $Pb(NO_3)_2$. The corresponding theoretical concentrations of Cu^{2+} and Pb^{2+} were 50.9 ppm and 125.1 ppm, respectively. However, the actual initial concentrations of $MgCl_2$, Cu^{2+}, and Pb^{2+} were slightly lower than the above values because of a dilution of the feed and draw solutions with the residual DI water in the membrane cell and the pumps circulating the feed and draw solution [27].

The water flux (J_w) and the reverse draw solute flux (J_s) were evaluated from the respective steady-state mass transfer rates of water (dm_w/dt) and the draw solute (dm_s/dt):

$$J_w = \frac{dm_w/dt}{\rho A_m} \tag{1}$$

$$J_s = \frac{dm_s/dt}{A_m} \tag{2}$$

where ρ is the density of water and A is the membrane area. In the experiments with feed solution containing heavy metals, the solute and water permeate in the same direction. Therefore, the heavy metal rejection (R) is:

$$R = \left(1 - \frac{C_p}{C_f} \right) \tag{3}$$

where C_p and C_f are steady-state concentrations of heavy metal in permeate and feed, respectively. It is essential to remember that during experiments, both feed and draw solutions were circulated at the respective sides of the membrane while the water permeated from the feed to the draw side. Therefore, in principle, no steady state could be attained. However, since the volume of water that permeated across the membrane was negligible compared to the volumes of feed and draw solutions, a pseudo-steady state could be reached, which we will refer to as a steady state. The following section will show that the steady state existed almost instantaneously after the experiment's initiation. Since the initial concentration of heavy metal in the draw solution was zero, the C_p was evaluated from [28]:

$$C_p = \frac{C_{d,f} V_{d,f}}{\Delta V_d} \tag{4}$$

where: $C_{d,f}$, which is the concentration of heavy metal in the draw solution at the end of the experiment, and ΔV_d, which is the total volume of water permeated from the feed to the draw solution, were measured directly. The final volume of the draw solution at the end of the experiment ($V_{d,f}$) was estimated from [28]:

$$V_{d,f} = V_{d,i} + V_{d,r} + \Delta V_d \tag{5}$$

where: $V_{d,i}$ is the initial volume of the draw solution, which in every experiment was 840 mL, and $V_{r,d}$ is the residual volume of water in the draw-side of the system, which represents the volume of water in the tubing, the membrane cell, and the pump. The final volume of the feed solution ($V_{f,f}$) was estimated from a similar equation [28]:

$$V_{f,f} = V_{f,i} + V_{f,r} - \Delta V_d \tag{6}$$

where: $V_{f,i}$ is the initial volume of the feed solution, which in every experiment was 500 mL, and $V_{r,f}$ is the residual volume of water in the feed side of the system. The residual volumes of water at the draw and feed sides were $V_{r,d}$ = 161.5 mL and $V_{r,f}$ = 155.5 mL [26].

2.4. Rejection of Heavy Metals in NF Process

In addition to FO, the rejection of Cu^{2+} (200 ppm $CuSO_4 \cdot 5H_2O$ solution) was also measured in NF experiments. The tests were performed using the TFN and the control TFC membranes in a continuous crossflow filtration system [29]. The experiments were carried out at $24 \pm 2\,°C$ and 10 ± 1 bar. Heavy metal rejection was evaluated using Equation (3). Unlike FO tests, C_p and C_f were measured directly from the samples taken when steady-state permeation was established. The feed and permeate samples were analyzed using ICP-MS. Due to a large feed solution volume (~20 L), a decrease in C_f was not observed.

3. Results and Discussion

3.1. Nanoparticle and Membrane Characterization

The following summarizes the important properties of nanoparticles and the resulting TFN and TFC membranes described in detail previously [24]. These excerpts will help better understand this work's core results, i.e., the FO performance and how heavy metals influence this performance.

The successful functionalization of HNTs using the first-generation PAMAM dendrimers was confirmed by two additional characteristic peaks in the ATR-FTIR spectrum

of the functionalized HNTs. Based on the TGA analysis, the organic content resulting from the functionalization was approximately 5%. The TEM and SEM images revealed that nanoparticles are heterogeneous in size but have a characteristic tubular geometry. The variation in size could not be attributed to the functionalization of HNTs. On the other hand, the incorporation of the first-generation PAMAM dendrimers greatly affected the zeta potential of the nanoparticles. The zeta potential increased from -34.5 mV to 2.2 mV for the functionalized HNTs because of the presence of amino groups from the first generation of PAMAM dendrimers [24].

The formation of the active polyamide (PA) layer and incorporation of the nanoparticles into the PA layer were confirmed by the ATR-FTIR spectra. The relative intensity of the characteristic primary amide and aromatic amide peaks was greater in TFN than in the control TFC membrane. However, there was no clear trend between the peak intensity and the nanoparticle loading for the TFN membranes. The SEM images of the top surface of the membranes revealed a typical nodular structure. Incorporating the nanoparticles decreased the uniformity of the top surface because of the penetration of the nanoparticles and possible aggregation of HNTs at higher loadings. The water contact angle of TFN membranes was lower than that of control TFC membranes, and the increase in hydrophilicity was attributed to the hydroxyl and amine groups of the nanoparticles. However, the water contact angle did not continue to decrease with the nanoparticle loading. At the highest loading, the contact angle increased, likely because of the aggregation of some nanoparticles. Although the zeta potential of the HNTs functionalized with first-generation PAMAM dendrimers was slightly positive, their incorporation into the PA layer had little effect on the zeta potential of the resulting TFN membranes compared to the control TFC membrane [24].

3.2. FO Performance

The FO performance of the membranes strongly depends on a draw solute. The latter should generate high osmotic pressure while the permeation of salt across the membrane is minimized. In this study, we selected $MgCl_2$ as a draw solute because, as we have shown previously, our novel TFN-NF membranes have excellent rejection of $MgCl_2$ [24].

Figure 2 shows the progress of the dynamic FO experiments with the control TFC membrane using DI water and a 200 ppm $CuSO_4 \cdot 5H_2O$ as a feed solution. In both cases, 1 M aqueous solution of $MgCl_2$ was used as a draw solution. The processing of the raw experimental data was described elsewhere [26]. In both experiments, the rate of water mass change (dm_w/dt) is linear, indicating steady-state conditions right after the initiation of the experiment. It is important to note that the rate of the mass increase at the draw side is equal to the rate of the mass decrease at the feed side, as it should be. It is because the FO system is closed, and the total mass of water is constant. The water transport from the feed to the draw side decreases the concentration of the draw solute, and thus, the driving force for the water transport decreases during the experiment. However, because the total mass of water transferred over an hour-long experiment (<10 g) was much smaller than the total mass of either feed (~500 g) or draw solution (~840 g), the osmotic pressure gradient remained constant.

The most remarkable observation from Figure 2 is that the slope of the rate of mass change, i.e., J_w, was 50% greater in the experiment with the feed solution containing 200 ppm $Pb(NO_3)_2$ than in the one with DI water as a feed solution. In principle, heavy metal salt in the feed solution decreases the osmotic pressure difference across the membrane. As a result, one could expect the water flux in the experiment with pure water to be higher than in the experiment with a heavy metal salt solution in the feed.
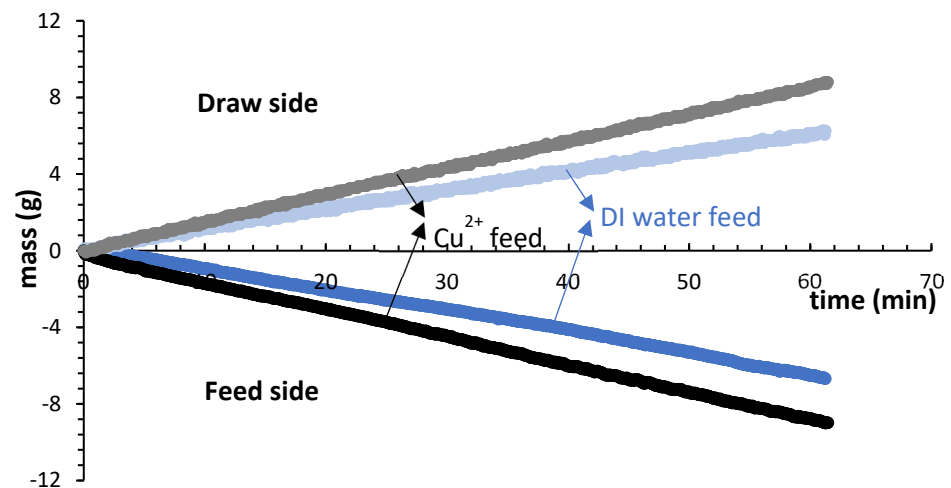
Figure 2. Progress of dynamic FO experiments using a TFC membrane in the AL-FS orientation; the mass of the feed and draw solutions as a function of time. Draw solution: 1 M MgCl$_2$; feed solution: DI water or aqueous 200 ppm CuSO$_4$·5H$_2$O solution. Temperature: 24 °C.

Figure 3 presents the progress of the same dynamic FO experiments with the TFC membrane focusing on the reverse salt flux of the draw solute (MgCl$_2$) as a function of time. Unlike the water flux, it takes several minutes for MgCl$_2$ transport to become constant, particularly in the experiment with DI water as a feed. The most remarkable result in Figure 3 is markedly smaller J_s of MgCl$_2$ in the experiment with the feed solution containing the heavy metal salt. Heavy metal ions in the feed solution appear to suppress the reverse of MgCl$_2$, which is desirable.
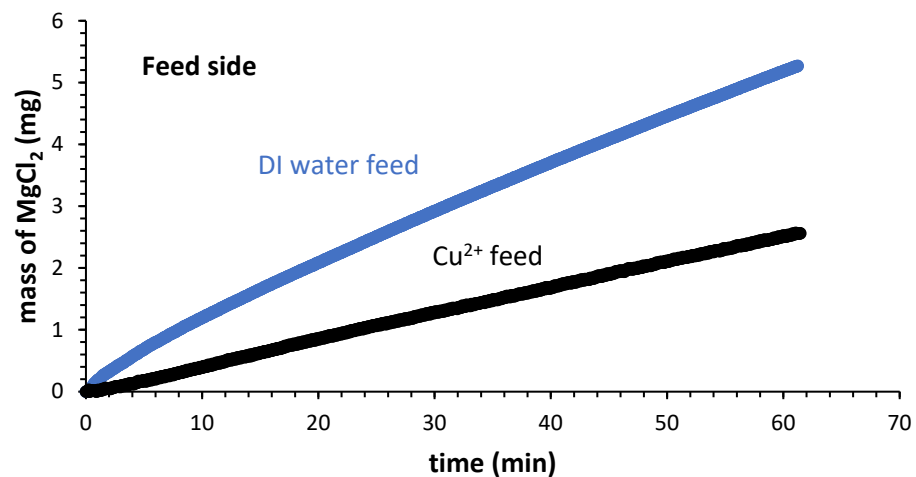

Figure 3. Progress of dynamic FO experiments using a TFC membrane in the AL-FS orientation; the mass of MgCl$_2$ as a function of time. Draw solution: 1 M MgCl$_2$; feed solution: DI water or aqueous 200 ppm CuSO$_4$·5H$_2$O solution. Temperature: 24 °C.

When analyzing the experiment results with the feed containing 200 ppm CuSO$_4$·5H$_2$O, we assumed that the membrane completely rejects the heavy metal ions. In other words, the feed solution's conductivity changes are solely determined by the transport of MgCl$_2$ from the draw to the feed solution. One of the concerns with using MgCl$_2$ as a draw solute was its incomplete rejection by our membranes in the NF experiments [24]. However, heavy metal salt in the feed solution significantly alleviates this problem.

The FO tests, similar to those summarized in Figures 2 and 3, were also performed with TFN membranes, and the results for the water flux (J_w) and reverse solute flux (J_s) are shown in Figures 4 and 5, respectively. For each loading of nanoparticles, including

zero loading, i.e., TFC membranes, we prepared two membrane sheets, and we cut four coupons from each sheet. Therefore, in total, we fabricated 32 coupons for the FO tests. The bars representing J_w and J_s in the experiments with DI water as a feed solution are the average from tests using four coupons of the same membrane type. For the experiments with the feed solution containing $Pb(NO_3)_2$ or $CuSO_4 \cdot 5H_2O$, the bars are the average from tests using two coupons of the same type of membrane.
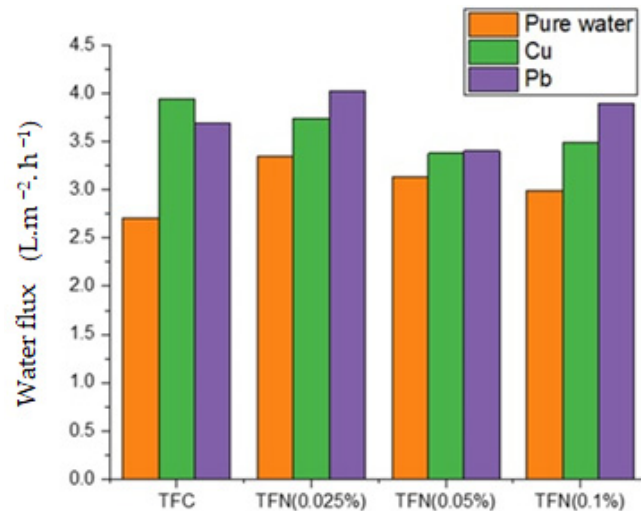

Figure 4. The average water flux of TFC and TFN membranes using the different feed solutions. Orange: DI water; green: 200 ppm $CuSO_4 \cdot 5H_2O$ solution; purple: 200 ppm $Pb(NO_3)_2$ solution. Draw solution in all experiments: 1 mol/L $MgCl_2$.

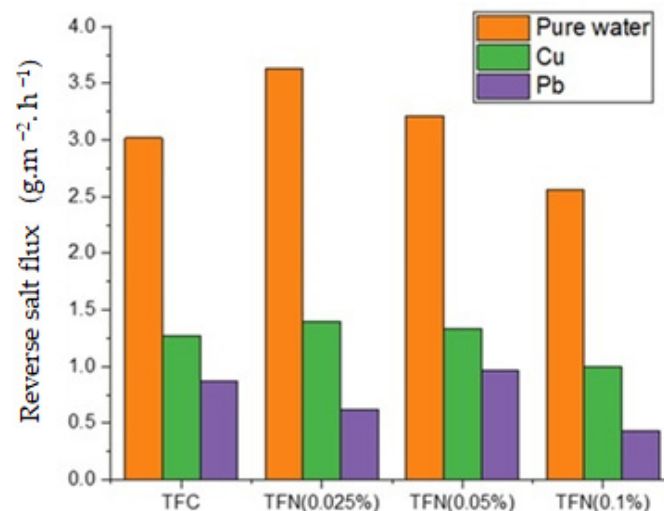**Figure 5.** The average reverse flux of $MgCl_2$ of TFC and TFN membranes using the different feed solutions. Orange: DI water; green: 200 ppm $CuSO_4 \cdot 5H_2O$ solution; purple: 200 ppm $Pb(NO_3)_2$ solution. Draw solution in all experiments: 1 mol/L $MgCl_2$.

Figure 4 confirms that heavy metal salt in the feed solution enhances the water flux. For TFC membranes, the water flux increases in the following: DI water < $Pb(NO_3)_2$ solution < $CuSO_4 \cdot 5H_2O$ solution. For TFN membranes, the water flux for the $Pb(NO_3)_2$ solution is higher than for the $CuSO_4 \cdot 5H_2O$ solution. However, the positive effect of the heavy metal in the feed on the water flux is undeniable. The water fluxes of less than $4\,L \cdot m^{-2} \cdot h^{-1}$ are relatively low for the FO process. Nonwoven support, a part of commercial PS35 membranes on which TFC and TFN membranes were synthesized, is responsible for internal concentration polarization (ICP). The latter significantly reduces the effective

osmotic pressure gradient, the driving force for water transport in FO processes [15]. There is no clear trend between the water flux and the loading of HNT-G1.

As shown in Figure 5, the effect of heavy metal cations in the feed solution on the reverse flux of $MgCl_2$ is much stronger than that on the water flux. The reduction in the reverse salt flux in the presence of heavy metal ions is at least 50%, but it can also be significantly greater. For example, for TFN (0.1%), J_s in the presence of $Pb(NO_3)_2$ solution is 1/6 of that with DI water as a feed. For both TFC and TFN membranes, the reverse $MgCl_2$ flux decreases in the following order DI water > $CuSO_4 \cdot 5H_2O$ solution > $Pb(NO_3)_2$ solution. Although the respective feed solutions concentrations containing heavy metal salts were the same (200 ppm), the theoretical concentration of Pb^{2+} was greater than that of Cu^{2+} (125.1 ppm vs. 50.9 ppm). The greater concentration of Pb^{2+} in the feed solution could be responsible for the more significant reduction in J_s in the presence of $Pb(NO_3)_2$ in the feed solution. Considering the effect of loading of HNTs-G1 and the reverse salt flux, J_s decreases with the loading of HNTs-G1 when the feed solution is DI water and the aqueous solution of $CuSO_4 \cdot 5H_2O$. On the other hand, the is no clear trend between the loading and J_s when the feed solution contains the aqueous solution of $Pb(NO_3)_2$. It is also important to note that the reverse salt flux of TFC membrane is comparable to that of the TFN (0.025%) membrane.

The surface of fresh TFC and TFN membranes was negatively charged [24], which can be attributed to carboxylic acid groups from the unreacted acyl chloride of the TMC monomer [30]. Consequently, they can adsorb positively charged ions such as Pb^{2+} and Cu^{2+} [31]. According to Hurwitz et al. [32], adsorbed heavy metal ions on a solid surface can produce a strong hydration force, increasing the hydrophilicity. It is well known that the water flux increases as the surface hydrophilicity of membranes increases. In addition, adsorbed Cu^{2+} or Pb^{2+} would facilitate the rejection of Mg^{2+} cations based on charge repulsion. To maintain the electroneutrality, Cl^- anions would remain at the draw side of the membrane [33].

To confirm the adsorption of heavy metal ions on the membrane surface, we performed the ICP-MS analysis of the selected membranes (TFC and TFN (0.025%)) after the experiments with the feed solution containing $CuSO_4 \cdot 5H_2O$. For comparison, we also performed an ICP analysis of the same type of membranes after the experiments with DI water as a feed solution. In addition, we also measured the zeta potential of these membranes before and after the FO experiments. Table 1 summarizes the ICP and zeta potential analysis results.

Table 1. Summary of the ICP analysis and zeta potential analysis of selected membranes before and after the FO experiments.

Membrane	Initial Zeta Potential (mV)	Final Zeta Potential (mV)		Adsorbed Cu^{2+} (µg)	
		DI Water Feed	Cu^{2+} in Feed	DI Water Feed	Cu^{2+} in Feed
TFC	−17.8	−10.2	−8.72	1.27	8.83
TFN (0.25%)	−20.1	−15.5	−14.5	8.39	10.41

As expected, copper was detected on both TFC and TFN (0.025%) membranes after the tests with a feed solution containing $CuSO_4 \cdot 5H_2O$. Interestingly, copper was also detected on these membranes after the tests with DI water as a feed solution, particularly on the TFN (0.025%) membrane. The latter was likely because of residual heavy metal salts that had accumulated in the system, particularly in the membrane cell. On the other hand, more copper was detected after the tests, with the feed solution containing more $CuSO_4 \cdot 5H_2O$ than after the tests with DI. Because of possible contamination from the previous tests, the mass of copper reported in Table 1 should not be considered quantitatively. Nevertheless, the ICP analysis provides strong evidence for the adsorption of heavy metals on our TFC and TFN membranes. The adsorption of Cu^{2+} (and also Pb^{2+}) by membranes can be attributed to the chelation reaction of amine groups with heavy metal cations [34].

Further confirmation for the membrane adsorption of heavy metal ions comes from analyzing the zeta potential results. As shown in Table 1, the zeta potential of the new TFC membrane was -17.8 mV. After the test with DI water as a feed solution, the zeta potential decreased to -10.2 mV; however, after the test with the 200 ppm $CuSO_4 \cdot 5H_2O$ solution as a feed, the zeta potential increased further, to -8.72 mV. The same trend was observed for the TFN (0.025%) membrane. A zeta potential increase is attributed to the adsorption of metal cations. The zeta potential increase after the tests with DI water was likely because of Mg^{2+} adsorption from the draw solution. It is important to emphasize that surface zeta potential is sensitive to the pH of the environment. As pH increases, the zeta potential increases (becomes less negative) [35].

3.3. Rejection of Heavy Metals in FO and NF Processes

The presence of heavy metal cations in feed solution improves the FO performance of TFC and TFN membranes. However, the membrane's primary role in the FO process is to reject heavy metals while allowing water to permeate from the feed to the draw solution. The rejection of Cu^{2+} and Pb^{2+} was calculated using Equation (3), in which C_p was evaluated using Equation (4). The latter equation assumes that the initial concentration of Cu^{2+} and Pb^{2+} in the draw solution was zero, which was the case, and the existence of steady-state permeation during the entire FO experiment. The linear rate of mass change of water (Figure 2) and practically linear rate of mass change of heavy metal cations in the draw solution (Figure 3) confirmed the existence of steady-state conditions throughout the experiments.

To calculate R we used C_f measured after the experiment, which ranged from 34 to 36 ppm for Cu^{2+} and 77 to 92 ppm for Pb^{2+}. These values are lower than the respective theoretical concentrations of Cu^{2+} and Pb^{2+} that consider the dilution factor (0.5/0.656), i.e., 39 ppm and 95 ppm. The corresponding C_p values for Cu^{2+} ranged from 0.5 to 1.5 ppm and from 2 and 5 ppm for Pb^{2+}. The higher concentration of Pb^{2+} compared to Cu^{2+} was because of the higher C_f of the former. Using C_f measured after the experiment to calculate ion rejection lead to a conservative estimation of R values.

Figure 6 summarizes the average rejections of Cu^{2+} and Pb^{2+} by TFC and TFN membranes in FO tests. Each value in Figure 6 represents the average from two independent experiments. It can be observed that the average rejection of Pb^{2+} by TFC membrane (97.4%) is higher than Cu^{2+} (96%). On the other hand, for TFN membranes, the situation is the opposite; the average rejection of Cu^{2+} by TFN membranes (97.2–98.1%) is higher than Pb^{2+} (94.5–96%). The presence of HNTs-G1 slightly increases the rejection of Cu^{2+} of the resulting TFN, but the opposite is true for Pb^{2+}. However, there is no apparent trend between the loading of HNTs-G1 and heavy metal rejection by the membranes. Although differences in heavy metal rejections in Figure 6 might not be statistically significant, they are high—above 94.5%.

A different effect of incorporating HNTs-G1 into the TFN membranes on rejecting Cu^{2+} and Pb^{2+} might be related to a slight decrease in the surface zeta potential of the resulting TFN membrane (Table 1). TFC and TFN membranes used in this study had a negative surface zeta potential. Therefore, they were repelling anions apart from adsorbing positively charged Cu^{2+} and Pb^{2+}. The greater the valence of the anion, the stronger the repulsion. In other words, SO_4^{2-} should be better rejected than NO_3^{-}. Combined with the principle of electroneutrality, this explains the generally higher rejection of Cu^{2+} associated with SO_4^{2-} than Pb^{2+} associated with NO_3^{-}.

As shown in Table 1, high rejections of Cu^{2+} and Pb^{2+} might be partly due to the adsorption of heavy metal ions by the negatively charged surface of TCF and TFN membranes and/or HNTs-G1 nanoparticles. In principle, the adsorption of heavy metals by the membranes (m_{ads}) could be evaluated from the mass balance using the following equation:

$$m_{ads} = C_{f,i}V_{f,i} - C_p\Delta V_d - C_{f,f}\left(V_{f,i} - \Delta V_d + V_{r,f}\right) \tag{7}$$
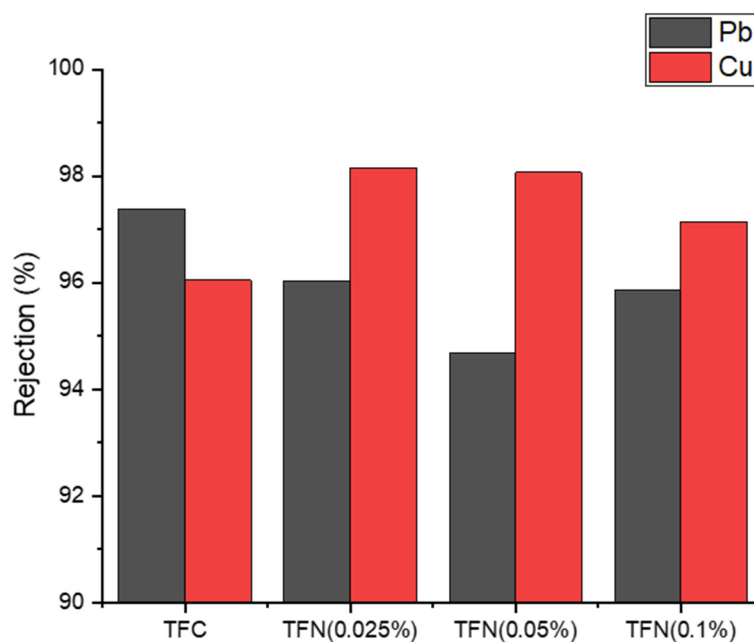
Figure 6. The average rejections of Cu^{2+} and Pb^{2+} by TFC and TFN membranes in FO tests.

All parameters on the right-hand side of Equation (7) were measured or evaluated in each experiment. However, the calculated m_{ads} were 2–3 orders of magnitude greater than the values reported in Table 1. The main reason for this discrepancy was the assumption that the membranes only adsorbed heavy metal ions. However, they could also be adsorbed in tubes and the membrane cell. In other words, in reality, there is another negative term on the right-hand side of Equation (7). The hypothesis of possible adsorption of heavy metal ions not only by the membranes was confirmed by the presence of Cu^{2+} on the membranes even in the experiments in which the feed solution was DI water (Table 1). However, it is essential to emphasize that the possible adsorption of heavy metal ions in the system and their incomplete removal between the experimental runs do not affect the calculation of *R* values.

In addition to rejecting heavy metals in FO experiments, we tested six TFC and six TFN (0.05%) membranes in NF experiments with a 200 ppm $CuSO_4 \cdot 5H_2O$ feed solution at 10 bar. The average rejection of Cu^{2+} by the TFC membranes was 96.25%, comparable to the corresponding value in the FO tests. On the other hand, the average rejection of Cu^{2+} by the TFN (0.05) membranes was only 92.89%, considerably lower than 98% by the same membranes in the FO tests. A lower rejection of heavy metals in NF compared to FO could be expected. In both processes, the transport of heavy metals is driven by the concentration gradient across the membrane. In addition, heavy metals might also be dragged along the permeating water in the NF process driven by the hydraulic pressure gradient across the membrane.

The FO performance, including the heavy metal ion rejection of TFC and TFN membranes, is generally comparable. This suggests a minor role of HNTs-G1, further substantiated by a general lack of trend between the nanoparticle loading and the membrane performance. A significant reduction in the reverse salt flux and the simultaneous increase in the water flux in the presence of heavy metal ions in the feed solution, attributed to their adsorption, is likely due to the negative surface charge of both TFC and TFN membranes rather than the adsorption by HNTs-G1. Two approaches are possible to increase the adsorption of heavy metals by the membranes and further improve their FO performance and heavy metal rejection. One method is to use nanoparticles, which would increase the negative surface charge of the final TFN membranes. For example, carboxyl group-grafted molybdenum disulfide [36] or silver-functionalized biomimetic nanoparticles could be used [37]. However, increasing the negative surface charge of the membranes could

deteriorate the rejection of $MgCl_2$. Consequently, a better approach would be to select nanoparticles that specifically interact with heavy metal ions. The thiol (SH) functional groups enhance heavy metal adsorption through complexation [38]. They can be introduced into TFN membranes via, for example, L-cysteine functionalized cellulose nanocrystals [35]. Despite an increase in the FO water flux in the presence of heavy metal ions, the reported J_s in Figure 4 remains small because of the ICP. The latter arises from the nonwoven support of the commercial PS35 membranes used to fabricate the TFC and TFN membranes. Increasing J_w to an attractive level for a practical FO application would require optimizing the porous support of the TFC and TFN membranes [39].

4. Conclusions

We have successfully fabricated thin-film nanocomposite (TFN) membranes through in situ interfacial polymerization of piperazine (PIP) and 1,3,5-benzenetricarbonyl trichloride (TMC) containing different amounts of functionalized halloysite nanotubes (HNTs) nanoparticles. The HNTs nanoparticles were functionalized with the first generation of poly(amidoamine) (PAMAM) dendrimers. These membranes demonstrated excellent rejection of heavy metal ions, specifically Cu^{2+} and Pb^{2+}, ranging from 94.5% to 98.1%. Interestingly, the TFN membranes exhibited higher rejection of Cu^{2+} compared to Pb^{2+}, while the opposite trend was observed for the control TFC membranes. In addition, the presence of heavy metals in the feed solution improved the performance of all membranes in the forward osmosis (FO) process, resulting in at least a 2.5-fold decrease in the reverse flux of draw solute ($MgCl_2$) and an increase in water flux. This improved performance is attributed to the adsorption of heavy metals by the membranes, as confirmed by the decrease in the negativity of zeta potential and the results from inductively coupled plasma mass spectrometry (ICP-MS) analysis of the membranes. The performance of TFN and TFC membranes, including heavy metal ion rejection, was generally comparable, indicating a minor role of HNTs-G1 nanoparticles. Therefore, to further improve the FO performance and heavy metal rejection, it is recommended to use nanoparticles that would increase the negative surface charge of the resulting TFN membranes or could specifically adsorb heavy metal ions. In addition, in the next phase of this research, it is recommended to use the actual wastewater as a feed to consider the role of organic matter when removing Cu^{2+} and Pb^{2+} ions in the FO process.

Author Contributions: Conceptualization, B.K.; Methodology, A.A., D.E. and B.K.; Validation, A.A.; Formal analysis, A.A.; Investigation, A.A. and D.E.; Resources, B.K.; Data curation, D.E.; Writing—original draft, A.A.; Writing—review & editing, D.E. and B.K.; Supervision, B.K.; Project administration, B.K.; Funding acquisition, B.K. All authors have read and agreed to the published version of the manuscript.

Data Availability Statement: We can make the data available upon request.

References

1. Cheng, X.; Zhang, Y.; Shao, S.; Lai, C.; Wu, D.; Xu, J.; Luo, X.; Xu, D.; Liang, H.; Zhu, X. Highly Permeable Positively Charged Nanofiltration Membranes with Multilayer Structures for Multiple Heavy Metal Removals. *Desalination* **2023**, *548*, 116266. [CrossRef]
2. Hübner, R.; Astin, K.B.; Herbert, R.J.H. "Heavy Metal"—Time to Move on from Semantics to Pragmatics? *J. Environ. Monit.* **2010**, *12*, 1511–1514. [CrossRef]
3. Fu, F.; Wang, Q. Removal of Heavy Metal Ions from Wastewaters: A Review. *J. Environ. Manag.* **2011**, *92*, 407–418. [CrossRef] [PubMed]
4. Abdullah, N.; Yusof, N.; Lau, W.J.; Jaafar, J.; Ismail, A.F. Recent Trends of Heavy Metal Removal from Water/Wastewater by Membrane Technologies. *J. Ind. Eng. Chem.* **2019**, *76*, 17–38. [CrossRef]
5. Barakat, M.A. New Trends in Removing Heavy Metals from Industrial Wastewater. *Arab. J. Chem.* **2011**, *4*, 361–377. [CrossRef]

6. Giwa, A.; Dindi, A.; Kujawa, J. Membrane Bioreactors and Electrochemical Processes for Treatment of Wastewaters Containing Heavy Metal Ions, Organics, Micropollutants and Dyes: Recent Developments. *J. Hazard. Mater.* **2019**, *370*, 172–195. [CrossRef] [PubMed]

7. Upadhyay, U.; Sreedhar, I.; Singh, S.A.; Patel, C.M.; Anitha, K.L. Recent Advances in Heavy Metal Removal by Chitosan Based Adsorbents. *Carbohydr. Polym.* **2021**, *251*, 117000. [CrossRef] [PubMed]

8. Fei, Y.; Hu, Y.H. Recent Progress in Removal of Heavy Metals from Wastewater: A Comprehensive Review. *Chemosphere* **2023**, *335*, 139077. [CrossRef] [PubMed]

9. Su, J.; Yang, Q.; Teo, J.F.; Chung, T.S. Cellulose Acetate Nanofiltration Hollow Fiber Membranes for Forward Osmosis Processes. *J. Memb. Sci.* **2010**, *355*, 36–44. [CrossRef]

10. Ma, A.; Abushaikha, A.; Allen, S.J.; McKay, G. Ion Exchange Homogeneous Surface Diffusion Modelling by Binary Site Resin for the Removal of Nickel Ions from Wastewater in Fixed Beds. *Chem. Eng. J.* **2019**, *358*, 1–10. [CrossRef]

11. Samavati, Z.; Samavati, A.; Goh, P.S.; Fauzi Ismail, A.; Sohaimi Abdullah, M. A Comprehensive Review of Recent Advances in Nanofiltration Membranes for Heavy Metal Removal from Wastewater. *Chem. Eng. Res. Des.* **2023**, *189*, 530–571. [CrossRef]

12. Zhang, Y.; Zhang, S.; Gao, J.; Chung, T.S. Layer-by-Layer Construction of Graphene Oxide (GO) Framework Composite Membranes for Highly Efficient Heavy Metal Removal. *J. Memb. Sci.* **2016**, *515*, 230–237. [CrossRef]

13. Suhalim, N.S.; Kasim, N.; Mahmoudi, E.; Shamsudin, I.J.; Mohammad, A.W.; Zuki, F.M.; Jamari, N.L.A. Rejection Mechanism of Ionic Solute Removal by Nanofiltration Membranes: An Overview. *Nanomaterials* **2022**, *12*, 437. [CrossRef] [PubMed]

14. Peydayesh, M.; Mohammadi, T.; Nikouzad, S.K. A Positively Charged Composite Loose Nanofiltration Membrane for Water Purification from Heavy Metals. *J. Memb. Sci.* **2020**, *611*, 118205. [CrossRef]

15. Abdullah, W.N.A.S.; Tiandee, S.; Lau, W.; Aziz, F.; Ismail, A.F. Potential Use of Nanofiltration Like-Forward Osmosis Membranes for Copper Ion Removal. *Chin. J. Chem. Eng.* **2020**, *28*, 420–428. [CrossRef]

16. Wang, Y.N.; Goh, K.; Li, X.; Setiawan, L.; Wang, R. Membranes and Processes for Forward Osmosis-Based Desalination: Recent Advances and Future Prospects. *Desalination* **2018**, *434*, 81–99. [CrossRef]

17. Suwaileh, W.A.; Johnson, D.J.; Sarp, S.; Hilal, N. Advances in Forward Osmosis Membranes: Altering the Sub-Layer Structure via Recent Fabrication and Chemical Modification Approaches. *Desalination* **2018**, *436*, 176–201. [CrossRef]

18. Zhu, L.; Ding, C.; Zhu, T.; Wang, Y. A Review on the Forward Osmosis Applications and Fouling Control Strategies for Wastewater Treatment. *Front. Chem. Sci. Eng.* **2022**, *16*, 661–680. [CrossRef]

19. Singh, S.K.; Sharma, C.; Maiti, A. A Comprehensive Review of Standalone and Hybrid Forward Osmosis for Water Treatment: Membranes and Recovery Strategies of Draw Solutions. *J. Environ. Chem. Eng.* **2021**, *9*, 105473. [CrossRef]

20. Ghanbari, M.; Emadzadeh, D.; Lau, W.J.; Riazi, H.; Almasi, D.; Ismail, A.F. Minimizing Structural Parameter of Thin Film Composite Forward Osmosis Membranes Using Polysulfone/Halloysite Nanotubes as Membrane Substrates. *Desalination* **2016**, *377*, 152–162. [CrossRef]

21. Emadzadeh, D.; Ghanbari, M.; Lau, W.J.; Rahbari-Sisakht, M.; Matsuura, T.; Ismail, A.F.; Kruczek, B. Solvothermal Synthesis of Nanoporous TiO$_2$: The Impact on Thin-Film Composite Membranes for Engineered Osmosis Application. *Nanotechnology* **2016**, *27*, 345702. [CrossRef]

22. Abdullah, W.N.A.S.; Lau, W.J.; Aziz, F.; Emadzadeh, D.; Ismail, A.F. Performance of Nanofiltration-Like Forward-Osmosis Membranes for Aerobically Treated Palm Oil Mill Effluent. *Chem. Eng. Technol.* **2018**, *41*, 303–312. [CrossRef]

23. Setiawan, L.; Wang, R.; Li, K.; Fane, A.G. Fabrication of Novel Poly(Amide-Imide) Forward Osmosis Hollow Fiber Membranes with a Positively Charged Nanofiltration-like Selective Layer. *J. Memb. Sci.* **2011**, *369*, 196–205. [CrossRef]

24. Atashgar, A.; Emadzadeh, D.; Akbari, S.; Kruczek, B. Incorporation of Functionalized Halloysite Nanotubes (HNTs) into Thin-Film Nanocomposite (TFN) Nanofiltration Membranes for Water Softening. *Membranes* **2023**, *13*, 245. [CrossRef] [PubMed]

25. Shahamati Fard, F.; Akbari, S.; Pajootan, E.; Arami, M. Enhanced Acidic Dye Adsorption onto the Dendrimer-Based Modified Halloysite Nanotubes. *Desalin. Water Treat.* **2016**, *57*, 26222–26239. [CrossRef]

26. Bai, D.; Asempour, F.; Kruczek, B. Can the Time-Lag Method Be Used for the Characterization of Liquid Permeation Membranes? *Chem. Eng. Res. Des.* **2020**, *162*, 228–237. [CrossRef]

27. Bai, D.; Kruczek, B. Effect of Membrane Orientation and Concentration of Draw Solution on the Behavior of Commercial Osmotic Membrane in a Novel Dynamic Forward Osmosis Tests. *Membranes* **2022**, *12*, 385. [CrossRef]

28. Atashgar, A. Incorporation of Functionalized Halloysite Nanotubes (HNTs) into Thin Film Nanocomposite (TFN) Nanofiltration Membranes for Heavy Metal Removal from Wastewaters. Master's Thesis, University of Ottawa, Ottawa, ON, Cananda, 2021.

29. Asempour, F.; Emadzadeh, D.; Matsuura, T.; Kruczek, B. Synthesis and Characterization of Novel Cellulose Nanocrystals-Based Thin Film Nanocomposite Membranes for Reverse Osmosis Applications. *Desalination* **2018**, *439*, 179–187. [CrossRef]

30. Tul Muntha, S.; Kausar, A.; Siddiq, M. Advances in Polymeric Nanofiltration Membrane: A Review. *Polym. Plast. Technol. Eng.* **2017**, *56*, 841–856. [CrossRef]

31. Madaeni, S.S.; Salehi, E. Adsorption of Cations on Nanofiltration Membrane: Separation Mechanism, Isotherm Confirmation and Thermodynamic Analysis. *Chem. Eng. J.* **2009**, *150*, 114–121. [CrossRef]

32. Hurwitz, G.; Guillen, G.R.; Hoek, E.M.V. Probing Polyamide Membrane Surface Charge, Zeta Potential, Wettability, and Hydrophilicity with Contact Angle Measurements. *J. Memb. Sci.* **2010**, *349*, 349–357. [CrossRef]

33. Akharame, M.O.; Fatoki, O.S.; Opeolu, B.O. *Regeneration and Reuse of Polymeric Nanocomposites in Wastewater Remediation: The Future of Economic Water Management*; Springer: Berlin/Heidelberg, Germany, 2019; Volume 76, ISBN 0123456789.

34. Qiu, M.; He, C. Efficient Removal of Heavy Metal Ions by Forward Osmosis Membrane with a Polydopamine Modified Zeolitic Imidazolate Framework Incorporated Selective Layer. *J. Hazard. Mater.* **2019**, *367*, 339–347. [CrossRef] [PubMed]
35. Abedi, F.; Dubé, M.A.; Emadzadeh, D.; Kruczek, B. Improving Nanofiltration Performance Using Modified Cellulose Nanocrystal-Based TFN Membranes. *J. Memb. Sci.* **2023**, *670*, 121369. [CrossRef]
36. Wang, X.; Liu, Y.; Fan, K.; Cheng, P.; Xia, H.; Xia, S. Utilization of Carboxyl Group-Grafted Molybdenum Disulfide for Enhancing the Performance of Thin-Film Nanocomposite Nanofiltration Membranes. *Desalination* **2023**, *548*, 116283. [CrossRef]
37. Huo, H.Q.; Mi, Y.F.; Yang, X.; Lu, H.H.; Ji, Y.L.; Zhou, Y.; Gao, C.J. Polyamide Thin Film Nanocomposite Membranes with In-Situ Integration of Multiple Functional Nanoparticles for High Performance Reverse Osmosis. *J. Memb. Sci.* **2023**, *669*, 121311. [CrossRef]
38. Thabo, B.; Okoli, B.J.; Modise, S.J.; Nelana, S. Rejection Capacity of Nanofiltration Membranes for Nickel, Copper, Silver and Palladium at Various Oxidation States. *Membranes* **2021**, *11*, 653. [CrossRef]
39. Ang, W.L.; Wahab Mohammad, A.; Johnson, D.; Hilal, N. Forward Osmosis Research Trends in Desalination and Wastewater Treatment: A Review of Research Trends over the Past Decade. *J. Water Process Eng.* **2019**, *31*, 100886. [CrossRef]